All-Optical Optimal N-to-M Quantum Cloning of Coherent States

Shengshuai Liu,[1,*] Yanbo Lou,[1,*] Yingxuan Chen,[1] and Jietai Jing[1,2,3,†]
[1]State Key Laboratory of Precision Spectroscopy, Joint Institute of Advanced Science and Technology, School of Physics and Electronic Science, East China Normal University, Shanghai 200062, China
[2]Department of Physics, Zhejiang University, Hangzhou 310027, China
[3]Collaborative Innovation Center of Extreme Optics, Shanxi University, Taiyuan, Shanxi 030006, China

(Received 7 September 2020; revised 15 December 2020; accepted 15 January 2021; published 10 February 2021)

The laws of quantum mechanics forbid the perfect copying of an unknown quantum state, known as the no-cloning theorem. In spite of this, approximate cloning with imperfect fidelity is possible, which opens up the field of quantum cloning. In general, quantum cloning can be divided into discrete variable and continuous variable (CV) categories. In the CV regime, all-optical implementation of the optimal $N \rightarrow M$ quantum cloning has been proposed in two original parallel works, which involves a parametric amplifier and a set of beam splitters and thus avoids the optic-electro and electro-optic conversions in the current CV quantum cloning technologies. However, such original proposal of all-optical CV optimal $N \rightarrow M$ quantum cloning scheme has never been experimentally implemented. Here, we show that optimal $N \rightarrow M$ quantum cloning of coherent states can be realized by utilizing a parametric amplifier based on four-wave mixing process in a hot atomic vapor and a set of beam splitters. In particular, we realize $1 \rightarrow M$, $2 \rightarrow M$, and $4 \rightarrow M$ quantum cloning. We find that the fidelity of $N \rightarrow M$ quantum cloning increases with the decrease of clone number M and the increase of original replica number N. The best cloning fidelity achieved in our experiment is about 93.3% $\pm$1.0% in the $4 \rightarrow 5$ case. Our results may find potential applications in realizing all-optical high-fidelity quantum state transfer and all-optical high-compatibility eavesdropping attack in quantum communication networks.

DOI: 10.1103/PhysRevLett.126.060503

The foundation of quantum mechanics makes it impossible to clone an unknown quantum state perfectly [1,2]. However, this does not prohibit the imperfect cloning of an unknown quantum state, that is, approximate cloning. This enables the construction of quantum cloning machine, which is related to the security of quantum cryptography. After the quantum cloning machine was first theoretically proposed [3], it has been extensively and deeply studied at the aim of searching for the optimal quantum cloning machine [4]. In general, there are two categories of quantum cloning, i.e., discrete variable (DV) and continuous variable (CV) regimes. In DV regime, the fidelity of quantum cloning is related to the probability that the clone photon and the input photon are in the same state. The quantum state in DV quantum cloning is described by the physical quantity which has a discrete spectrum, such as polarization and orbital angular momentum. For example, the optimal DV quantum cloning machines have been implemented to clone quantum state encoded in the polarization [5–8] or orbital angular momentum [8–10] of photon.

Differently, the physical quantity, which has a continuous spectrum, is used to describe the quantum state in CV quantum cloning, such as amplitude quadrature and phase quadrature [11]. In this way, the quantum information of quantum state is also encoded in amplitude quadrature and phase quadrature of optical field in CV quantum cloning. CV cloning action will inevitably introduce additional noise to the input state. Such additional noise added to the amplitude quadrature and phase quadrature of the clone makes the perfect cloning impossible in CV regime. Therefore, the fidelity of CV quantum cloning, characterizing the similarity between the input and the clone, is related to the quadrature variances of input and clone at unity gain. In CV regime, the $1 \rightarrow M$ quantum cloning, which takes one original replica to produce M clones, has been studied in both theory [12] and experiment [13–15]. More generally, one can take N original replicas to produce M clones, realizing the so-called $N \rightarrow M$ quantum cloning. It has also been theoretically analyzed [16–18] and experimentally realized in the $2 \rightarrow 3$ case [19]. So far, all the experimental implementations of quantum cloning in CV regime rely on feed-forward and homodyne detection, which requests the optic-electro and electro-optic conversions [13–15,19]. While in the original proposal of optimal $N \rightarrow M$ quantum cloning in CV regime [17,18], its implementation is based on an all-optical architecture consisting of a parametric amplifier and a set of beam splitters (BSs) and thus avoids the optic-electro and electro-optic conversions in the current CV quantum cloning technologies. However, for its demonstration, a quantum limited linear amplifier, which is difficult to

implement [13], is needed. Therefore, such original proposal of optimal $N \to M$ quantum cloning in CV regime [17,18] has never been experimentally demonstrated, let alone to demonstrate its ability for efficiently enhancing cloning fidelity.

A four-wave mixing (FWM) process in an atomic vapor cell with a double-Λ energy level configuration [20–33] has been proved to be a near-quantum-limit low-noise amplifier [34,35] which is promising for realizing quantum cloning. In this Letter, by utilizing such linear amplifier based on FWM process, we experimentally realize the all-optical optimal N-to-M quantum cloning in CV regime. We experimentally show how the original replica number N and clone number M affect the fidelity of $N \to M$ quantum cloning. We find that both the increase of the original replica number N and the decrease of clone number M can enhance the cloning fidelity, which is consistent with the theoretical predictions.

The configuration of our all-optical optimal $N \to M$ quantum cloning scheme is shown in Fig. 1(a). N original replicas of coherent states are combined by $N-1$ BSs. After this operation, the energy of the N input coherent states are concentrated into one single field $\hat{a}_c$, which can be expressed as [17,18]

$$\hat{a}_c = \frac{1}{\sqrt{N}} \sum_{N=1}^{N} \hat{a}_{\mathrm{in},N}, \tag{1}$$

where $\hat{a}_{\mathrm{in},N}$ is the annihilation operator associated with input coherent state. Then, we seed this single field $\hat{a}_c$ and pump beam $\hat{c}$ into a linear amplifier based on FWM process. As shown in Fig. 1(b), this single (signal) field $\hat{a}_c$ are blueshifted from the pump beam. The amplified field $\hat{a}_{\mathrm{out}}$ after the FWM process can be described as

$$\hat{a}_{\mathrm{out}} = \sqrt{G}\hat{a}_c + \sqrt{G-1}\hat{b}^{\dagger}, \tag{2}$$

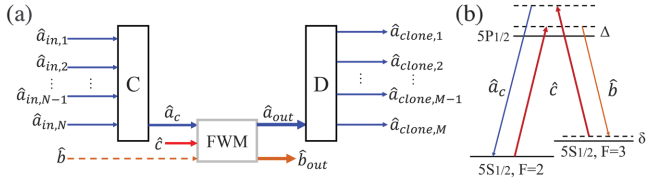

FIG. 1. The scheme of all-optical optimal N-to-M quantum cloning. (a) The schematic of $N \to M$ quantum cloning machine in CV regime. C, energy concentration operation; D, energy distribution operation; $\hat{a}_{\mathrm{in},1}, \ldots, \hat{a}_{\mathrm{in},N}$, original replicas; $\hat{a}_c$, energy-concentrated (signal) field; $\hat{b}$, idler field; $\hat{c}$, pump field; $\hat{a}_{\mathrm{out}}$ and $\hat{b}_{\mathrm{out}}$, output fields of the FWM process; $\hat{a}_{\mathrm{clone},1}, \ldots, \hat{a}_{\mathrm{clone},M}$, clones. All these field operators are annihilation operators associated with the corresponding optical fields. (b) Energy level diagram of ^{85}Rb $D1$ line for linear amplifier. Δ, one-photon detuning; δ, two-photon detuning.

where $\hat{b}$ (idler) is the vacuum input state of the FWM process. G is the intensity gain of the amplifier. In order to realize $N \to M$ quantum cloning, the gain of the FWM process should be equal to M/N. Therefore, $\hat{a}_{\mathrm{out}}$ can be expressed as

$$\hat{a}_{\mathrm{out}} = \frac{\sqrt{M}}{N} \sum_{N=1}^{N} \hat{a}_{\mathrm{in},N} + \sqrt{\frac{M}{N} - 1}\hat{b}^{\dagger}. \tag{3}$$

Then, $\hat{a}_{\mathrm{out}}$ is divided into M clones by $M-1$ BSs. Consequently, the clone can be written as

$$\hat{a}_{\mathrm{clone},l} = \frac{1}{\sqrt{M}}\hat{a}_{\mathrm{out}} + \hat{v}_l, \tag{4}$$

where $\hat{v}_l$ is the vacuum states introduced by BSs, $l = 1, \ldots, M$. The variance of $\hat{v}_l$ is $(M-1)/M$. Based on Eqs. (3) and (4), the clone $\hat{a}_{\mathrm{clone},l}$ can be given by

$$\hat{a}_{\mathrm{clone},l} = \frac{1}{N} \sum_{N=1}^{N} \hat{a}_{\mathrm{in},N} + \sqrt{\frac{1}{N} - \frac{1}{M}}\hat{b}^{\dagger} + \hat{v}_l. \tag{5}$$

The performance of the quantum cloning machine can be quantified by the overlap of the clone with the original replica, i.e., the fidelity. The fidelity of our all-optical optimal $N \to M$ quantum cloning can be given by

$$F = \frac{2}{\sqrt{(1 + \Delta^2 \hat{X}_{\mathrm{clone},l})(1 + \Delta^2 \hat{Y}_{\mathrm{clone},l})}}, \tag{6}$$

where $\hat{X}_{\mathrm{clone},l} = (\hat{a}_{\mathrm{clone},l} + \hat{a}^{\dagger}_{\mathrm{clone},l})$ and $\hat{Y}_{\mathrm{clone},l} = i(\hat{a}^{\dagger}_{\mathrm{clone},l} - \hat{a}_{\mathrm{clone},l})$ are the amplitude and phase quadratures of the clone $\hat{a}_{\mathrm{clone},l}$, respectively. $\Delta^2 \hat{X}_{\mathrm{clone},l}$ and $\Delta^2 \hat{Y}_{\mathrm{clone},l}$ denote the variances and read

$$\Delta^2 \hat{X}_{\mathrm{clone},l} = \Delta^2 \hat{Y}_{\mathrm{clone},l} = 1 + \frac{2}{N} - \frac{2}{M}. \tag{7}$$

Based on Eqs. (6) and (7), we can obtain the fidelity of $N \to M$ quantum cloning, which is given by

$$F = \frac{MN}{MN + M - N}. \tag{8}$$

From Eq. (8), it can be seen that for a given original replica number N, the fidelity of $N \to M$ quantum cloning increases as the decrease of the clone number M. Moreover, one can also find that the fidelity increases as the increase of the original replica number N for a given clone number M. It means that we can enhance the fidelity of quantum cloning by increasing the original replica number N or decreasing the clone number M. This clearly shows the advantage of $N \to M$ quantum cloning in terms of

enhancing cloning fidelity, which makes it possible to achieve near perfect cloning.

Our detailed experimental scheme for all-optical optimal $N \to M$ quantum cloning is shown in Fig. 2. The experiment starts from a cavity stabilized Ti:sapphire laser whose frequency is about 1 GHz blue detuned from the ^{85}Rb $D1$ line ($5S_{1/2}$, $F = 2 \to 5P_{1/2}$) as shown in Fig. 2(a). A polarization beam splitter (PBS) is used to divide the beam into two. The strong one, which is vertically polarized, is used as the pump beam of the linear amplifier. We pass the weak one through an acousto-optic modulator (AOM) to get a beam which is about 3.04 GHz blueshifted from the pump beam and horizontally polarized. Then, we modulate signals on the amplitude quadrature ($\hat{X}$) and the phase quadrature ($\hat{Y}$) of this horizontally polarized beam at 2 MHz radio frequency (rf) by using amplitude modulator (AM) and phase modulator (PM). After modulation, this beam is sent into the state preparation and energy concentration boxes, which are indicated by Figs. 2(b)–2(d) for $4 \to M$, $2 \to M$, and $1 \to M$ cases, respectively. For example, as shown in Fig. 2(b), for $4 \to M$ cloning, this beam is divided into four identical original replicas of coherent state by three 50:50 BSs, completing the state preparation. In other words, these four prepared original replicas are exactly the input states of the original proposal [18]. The intensity for each original replica is about 1 μW which corresponds to yellow trace in Fig. 3(a). Then, we use three 50:50 BSs to realize energy concentration operation. Both state preparation and energy concentration stages are indispensable for realizing $4 \to M$ quantum cloning [18]. Specifically, we combine two original replicas by BS1. The piezoelectric transducer (PZT) is placed in the path of one original replica to change the relative phase between these two original replicas. Their interference fringe is shown as the blue trace in Fig. 3(a). Its visibility is about 97%. After locking the relative phase with microcontrol unit (MCU) [32], the BS1 has one bright output and one vacuum output. In this way, the energy of these two original replicas are concentrated into one single beam, which is shown as the red trace in Fig. 3(a). Similarly, the energy of the other two original replicas are also concentrated into one single beam by BS2. Then, we combine the two bright output beams of BS1 and BS2 by BS3. Their interference fringe is shown as the green trace in Fig. 3(a). Its visibility is about 97%. Similarly, by relative phase locking, we completely accomplish the energy concentration for the four original replicas. The intensity of the energy-concentrated beam $\hat{a}_c$, which is shown as the black trace of Fig. 3(a), is almost four times of each original replica, indicating a good energy concentration examined by direct current (dc) component. In the meanwhile, we also examine the state preparation and the energy concentration of four original replicas at 2 MHz rf by balanced homodyne detection (BHD). The photodetector of BHD has a transimpedance gain of 10^5 V/A and a quantum efficiency of 97%. Its dc component is used to lock the phase of the BHD at 0 or $\pi/2$ by MCU to measure amplitude or phase quadrature of the optical field, respectively. The rf components from BHD are analyzed by spectrum analyzer (SA). First, as shown in Fig. 2(b), we insert five flip mirrors (FMs) to measure the variances of four original replicas at 2 MHz rf. By flipping up the five FMs (FM1–FM5) as needed, we inject the four original

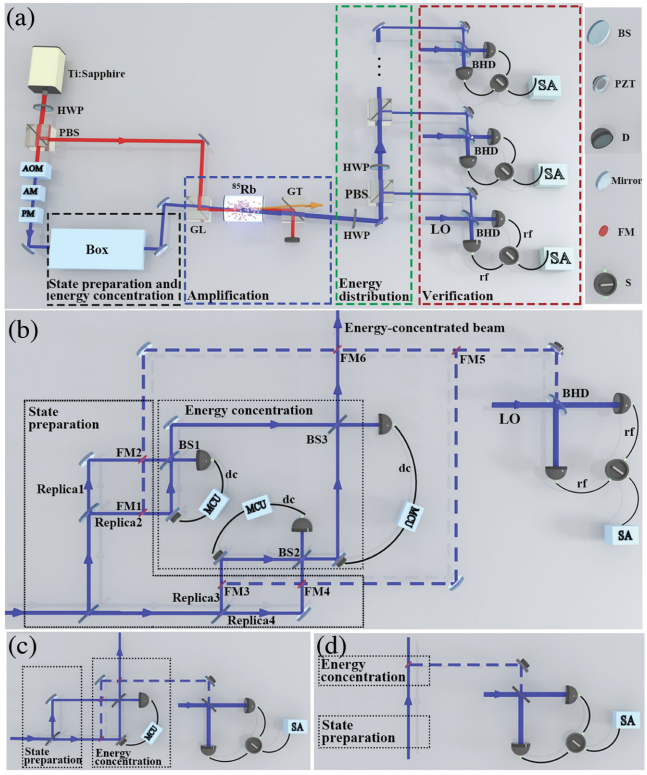

FIG. 2. The detailed experimental layout for N-to-M quantum cloning. (a) The detailed experimental scheme. State preparation and energy concentration for (b) $4 \to M$, (c) $2 \to M$, and (d) $1 \to M$ quantum cloning. HWP, half wave plate; PBS, polarization beam splitter; BS, beam splitter; AOM, acousto-optic modulator; AM, amplitude modulator; PM, phase modulator; FM, flip mirror; PZT, piezoelectric transducer; MCU, microcontrol unit; GL, Glan-Laser polarizer; GT, Glan-Thompson polarizer; BHD, balanced homodyne detection; D, photodetector; dc, direct current; rf, radio frequency; LO, local oscillator; S, subtractor; SA, spectrum analyzer; blue, signal beam; orange, idler beam; red, pump beam. The SA is set to a 30 kHz resolution bandwidth (RBW) and a 300 Hz video bandwidth (VBW). The LO beam with a power of 850 μW is obtained by setting up a similar FWM process. The seed of this FWM process is split from the beam right before the AM and after the AOM. In this way, the amplification of this seed produces the LO beam and its frequency naturally matches the frequencies of the replica, the energy-concentrated beam, and the clone. Then, we spatially mode match the LO beam to the replica, the energy-concentrated beam, and the clone under interrogation by adjusting its beam waist through choosing suitable lens combination. The visibilities of BHDs are all about 98%.

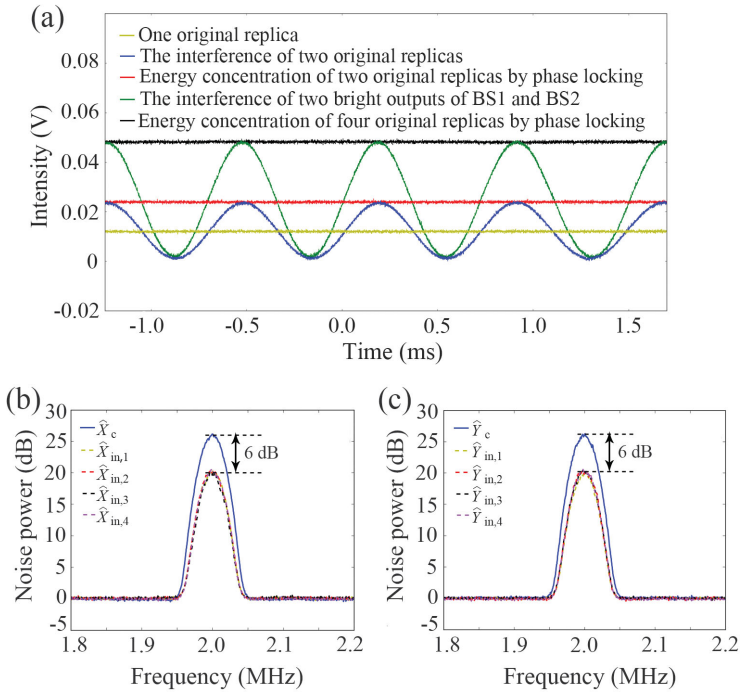

FIG. 3. Typical results of state preparation and energy concentration examined by (a) direct current component, (b) and (c) radio frequency mode for $4 \rightarrow M$ quantum cloning.

replicas into the same BHD, respectively. The measured results of amplitude quadrature and phase quadrature of the four original replicas are shown as the dashed lines in Figs. 3(b) and 3(c), respectively. We can see that the modulation signals of the amplitude quadrature $\hat{X}_{\text{in},1}$, $\hat{X}_{\text{in},2}$, $\hat{X}_{\text{in},3}$, $\hat{X}_{\text{in},4}$ (phase quadrature $\hat{Y}_{\text{in},1}$, $\hat{Y}_{\text{in},2}$, $\hat{Y}_{\text{in},3}$, $\hat{Y}_{\text{in},4}$) of the four original replicas are almost the same, demonstrating the accomplishment of state preparation at 2 MHz rf. Second, we insert another FM (FM6) to measure the variance of the energy-concentrated beam $\hat{a}_c$ at 2 MHz rf. By flipping up FM6, we inject the energy-concentrated beam into the same BHD as mentioned above. As shown in Figs. 3(b) and 3(c), the signal peaks at 2 MHz of the amplitude quadrature $\hat{X}_c$ [solid blue line in Fig. 3(b)] and the phase quadrature $\hat{Y}_c$ [solid blue line in Fig. 3(c)] of the energy-concentrated beam are about 6 dB above the corresponding results of the four original replicas. The value of 6 dB in logarithmic scale corresponds to four times in linear scale, showing the accomplishment of energy concentration at 2 MHz rf. These results prove that the state preparation and energy concentration examined by dc component is equivalent to the ones examined by rf mode for our all-optical quantum cloning machine. Combined by a Glan-Laser polarizer (GL), the energy-concentrated beam $\hat{a}_c$ and pump beam are crossed in the center of the ^{85}Rb vapor cell to realize linear amplification based on FWM process as shown in the amplification box of Fig. 2(a). Here, the energy-concentrated beam serves as the signal beam of the FWM process. The angle between the pump and energy-concentrated beams is about 7 mrad. The ^{85}Rb vapor cell is 12 mm long and its temperature is stabilized at 115 °C. The residual pump beam after the FWM process is eliminated by a Glan-Thompson polarizer (GT) with an extinction ratio of 10^5:1. After such amplification, the amplified signal beam $\hat{a}_{\text{out}}$ is obtained. Then, we send it into the energy distribution box for accomplishing quantum cloning as shown in Fig. 2(a). This amplified signal beam $\hat{a}_{\text{out}}$ is equally divided by a beam splitter network, which consists of M half wave plates (HWP) and M PBSs. Finally, the cloning fidelity is verified by BHD in verification box. This BHD is used for measuring the noise power spectra of the clone's amplitude and phase quadratures. Similarly, $2 \rightarrow M$ and $1 \rightarrow M$ all-optical optimal quantum cloning can be implemented by utilizing their own state preparation and energy concentration boxes as shown in Figs. 2(c) and 2(d), respectively.

The typical experimental results for $4 \rightarrow 16$ quantum cloning are shown in Fig. 4. As shown in Figs. 4(a) and 4(b), the blue (red) solid lines are the measured variances of amplitude quadrature and phase quadrature of one original replica (clone) with modulation signal at 2 MHz. The overlap between the modulation signal peaks of original replica and clone shows that the cloning gain is close to unity. It is also clear that additional noise has been added to the clone since the noise levels of the red solid lines are higher than the ones of the blue solid lines. In order to quantify the fidelity of the all-optical optimal $4 \rightarrow 16$ quantum cloning, we turn off the modulation signals of the original replicas and measure additional noise at 2 MHz introduced during the cloning operation. The blue (red)

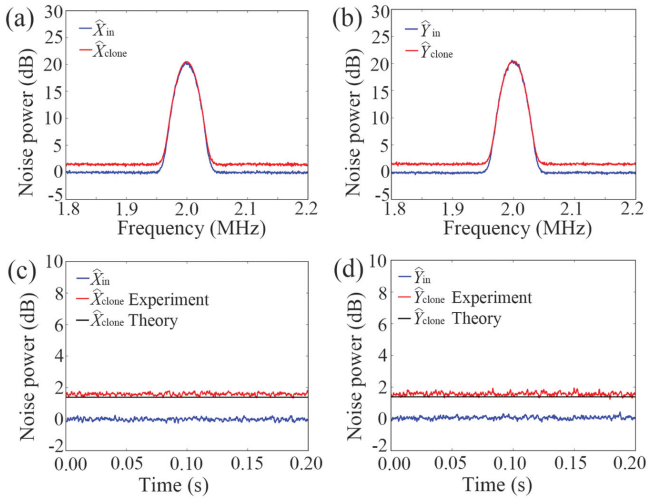

FIG. 4. The typical cloning results of amplitude quadrature [(a) and (c)] and phase quadrature [(b) and (d)] for the case of $4 \rightarrow 16$ with and without modulation signals.

solid lines in Figs. 4(c) and 4(d) are the noise levels of the amplitude and phase quadratures of one original replica (clone), respectively. The additional noises introduced by cloning are 1.60 ± 0.08 dB for amplitude quadrature and 1.50 ± 0.10 dB for phase quadrature, which corresponds to a cloning fidelity of 82.3% ±1.0%. The black straight lines are the corresponding theoretically predicted optimal cloning limits for the $4 \rightarrow 16$ case, which gives a fidelity (about 84.2%) close to the experimental value.

The fidelities of $1 \rightarrow M$, $2 \rightarrow M$, and $4 \rightarrow M$ all-optical optimal quantum cloning are shown in Fig. 5. First, we carry out $1 \rightarrow M$ quantum cloning with $M = 2, 3, 4$ by

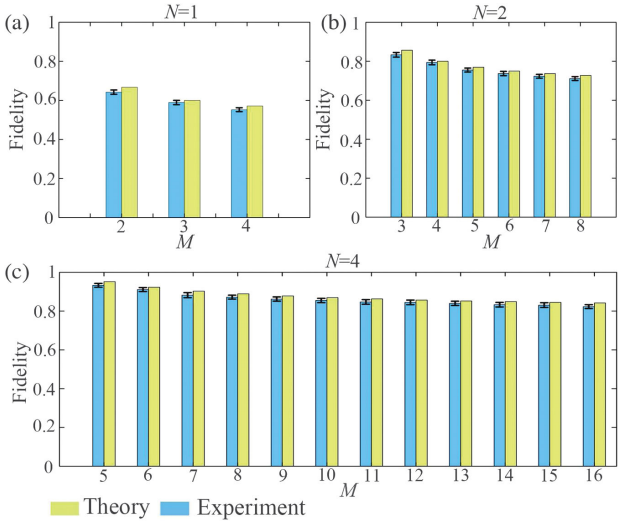

FIG. 5. The fidelities of $N \rightarrow M$ quantum cloning. (a) The fidelities of $1 \rightarrow M$ quantum cloning with $M = 2, 3, 4$. (b) The fidelities of $2 \rightarrow M$ quantum cloning with $M = 3, \ldots, 8$. (c) The fidelities of $4 \rightarrow M$ quantum cloning with $M = 5, \ldots, 16$. The error bars are obtained from the standard deviations of multiple repeated measurements.

varying the gain of the FWM process. As shown in Fig. 5(a), the corresponding experimental results (blue) and theoretical predictions (yellow) are very close and have the same trend as the increase of the clone number M. The best fidelity of $1 \rightarrow M$ quantum cloning is about 64.2% ±1.1%, which is achieved when $M = 2$, and is slightly lower than the theoretical value of $2/3$. Second, we implement $2 \rightarrow M$ quantum cloning with $M = 3, \ldots, 8$. The corresponding experimental results (blue) and theoretical predictions (yellow) are shown in Fig. 5(b). It can be seen that both the experimental and theoretical fidelities of $2 \rightarrow M$ quantum cloning decrease as the increase of the clone number M. The best fidelity of $2 \rightarrow M$ quantum cloning is about 83.3% ±1.2% in the case of $2 \rightarrow 3$. Third, we realize $4 \rightarrow M$ quantum cloning with $M = 5, \ldots, 16$ as shown in Fig. 5(c). The obtained fidelities of $4 \rightarrow M$ quantum cloning are all above 82%. The best fidelity of $4 \rightarrow M$ quantum cloning is about 93.3% ±1.0% for the case of $4 \rightarrow 5$ cloning. These results of Fig. 5 clearly show that the fidelity of $N \rightarrow M$ quantum cloning increases as the increase of the original replica number N. This is because the variances of the clones decrease with the increase of N as indicated by Eq. (7). Similarly, the increase of M increases the variances of the clones, which induces the decrease of the cloning fidelity.

In conclusion, we have experimentally implemented the all-optical optimal N-to-M quantum cloning in CV regime as proposed in the original works [17,18]. We find that for a given original replica number N, the fidelity of $N \rightarrow M$ quantum cloning increases with the decrease of clone number M. Moreover, we also find that for a given M, the fidelity of quantum cloning increases as the increase of N. Our results clearly show that our all-optical architecture based quantum cloning can efficiently enhance the cloning fidelity. The best cloning fidelity in our experiment is about $93.3\% \pm 1.0\%$ for the case of $4 \rightarrow 5$ quantum cloning. Our results may find potential applications in realizing all-optical high-fidelity quantum state transfer and all-optical high-compatibility eavesdropping attack in quantum communication networks.

This work was supported by the National Natural Science Foundation of China (11874155, 91436211, 11374104); Basic Research Project of Shanghai Science and Technology Commission (20JC1416100); Natural Science Foundation of Shanghai (17ZR1442900); Minhang Leading Talents (201971); Program of Scientific and Technological Innovation of Shanghai (17JC1400401); National Basic Research Program of China (2016YFA0302103); Shanghai Municipal Science and Technology Major Project (2019SHZDZX01); the 111 project (B12024).

*These authors contributed equally to this work.
†Corresponding author.
jtjing@phy.ecnu.edu.cn

[1] W. K. Wooters and W. H. Zurek, Nature (London) **299**, 802 (1982).
[2] D. Dieks, Phys. Lett. **92A**, 271 (1982).
[3] V. Buzek and M. Hillery, Phys. Rev. A **54**, 1844 (1996).
[4] V. Scarani, S. Iblisdir, N. Gisin, and A. Acín, Rev. Mod. Phys. **77**, 1225 (2005).
[5] A. Lamas-Linares, C. Simon, J. C. Howell, and D. Bouwmeester, Science **296**, 712 (2002).
[6] W. T. M. Irvine, A. L. Linares, M. J. A. de Dood, and D. Bouwmeester, Phys. Rev. Lett. **92**, 047902 (2004).
[7] S. Fasel, N. Gisin, G. Ribordy, V. Scarani, and H. Zbinden, Phys. Rev. Lett. **89**, 107901 (2002).
[8] E. Nagali, D. Giovannini, L. Marrucci, S. Slussarenko, E. Santamato, and F. Sciarrino, Phys. Rev. Lett. **105**, 073602 (2010).
[9] E. Nagali, L. S. Sciarrino, F. De Martini, L. Marrucci, B. Piccirillo, E. Karimi, and E. Santamato, Nat. Photonics **3**, 720 (2009).
[10] F. Bouchard, R. Fickler, and E. Karimi, Sci. Adv. **3**, e1601915 (2017).
[11] S. L. Braunstein and P. van Loock, Rev. Mod. Phys. **77**, 513 (2005).
[12] N. J. Cerf, A. Ipe, and X. Rottenberg, Phys. Rev. Lett. **85**, 1754 (2000).
[13] U. L. Andersen, V. Josse, and G. Leuchs, Phys. Rev. Lett. **94**, 240503 (2005).
[14] S. Koike, H. Takahashi, H. Yonezawa, N. Takei, S. L. Braunstein, T. Aoki, and A. Furusawa, Phys. Rev. Lett. **96**, 060504 (2006).
[15] J. Y. Haw, J. Zhao, J. Dias, S. M. Assad, M. Bradshaw, R. Blandino, T. Symul, T. C. Ralph, and P. K. Lam, Nat. Commun. **7**, 13222 (2016).
[16] N. J. Cerf and S. Iblisdir, Phys. Rev. A **62**, 040301(R) (2000).
[17] J. Fiurášek, Phys. Rev. Lett. **86**, 4942 (2001).
[18] S. L. Braunstein, N. J. Cerf, S. Iblisdir, P. van Loock, and S. Massar, Phys. Rev. Lett. **86**, 4938 (2001).
[19] M. Sabuncu, U. L. Andersen, and G. Leuchs, Phys. Rev. Lett. **98**, 170503 (2007).
[20] C. F. McCormick, V. Boyer, E. Arimonda, and P. D. Lett, Opt. Lett. **32**, 178 (2007).
[21] V. Boyer, A. M. Marino, R. C. Pooser, and P. D. Lett, Science **321**, 544 (2008).
[22] A. M. Marino, R. C. Pooser, V. Boyer, and P. D. Lett, Nature (London) **457**, 859 (2009).
[23] Q. Glorieux, L. Guidoni, S. Guibal, J.-P. Likforman, and T. Coudreau, Phys. Rev. A **84**, 053826 (2011).
[24] U. Vogl, R. T. Glasser, J. B. Clark, Q. Glorieux, T. Li, N. V. Corzo, and P. D. Lett, New J. Phys. **16**, 013011 (2014).
[25] M. W. Holtfrerich and A. M. Marino, Phys. Rev. A **93**, 063821 (2016).
[26] J. D. Swaim and R. T. Glasser, Phys. Rev. A **96**, 033818 (2017).
[27] S. Lohani and R. T. Glasser, Opt. Lett. **43**, 2611 (2018).
[28] M. Guo, H. Zhou, D. Wang, J. Gao, J. Zhang, and S. Zhu, Phys. Rev. A **89**, 033813 (2014).
[29] A. Kumar, H. Nunley, and A. M. Marino, Phys. Rev. A **95**, 053849 (2017).
[30] C. S. Embrey, M. T. Turnbull, P. G. Petrov, and V. Boyer, Phys. Rev. X **5**, 031004 (2015).
[31] B. J. Lawrie, P. G. Evans, and R. C. Pooser, Phys. Rev. Lett. **110**, 156802 (2013).
[32] S. Liu, Y. Lou, and J. Jing, Phys. Rev. Lett. **123**, 113602 (2019).
[33] R. C. Pooser, N. Savino, E. Batson, J. L. Beckey, J. Garcia, and B. J. Lawrie, Phys. Rev. Lett. **124**, 230504 (2020).
[34] R. C. Pooser, A. M. Marino, V. Boyer, K. M. Jones, and P. D. Lett, Phys. Rev. Lett. **103**, 010501 (2009).
[35] S. Liu, Y. Lou, and J. Jing, Nat. Commun. **11**, 3875 (2020).